Computer Methods in Applied Mechanics and Engineering 432 (2024) 117430

Contents lists available at ScienceDirect

Comput. Methods Appl. Mech. Engrg.

journal homepage: www.elsevier.com/locate/cma

Intrinsically selective mass scaling with hierarchic plate formulations

Lisa-Marie Krauß [a], Rebecca Thierer [a], Manfred Bischoff [a], Bastian Oesterle [b,*]

[a] University of Stuttgart, Institute for Structural Mechanics, Pfaffenwaldring 7, 70550 Stuttgart, Germany
[b] Hamburg University of Technology, Institute for Structural Analysis, Denickestraße 17, 21073 Hamburg, Germany

GRAPHICAL ABSTRACT

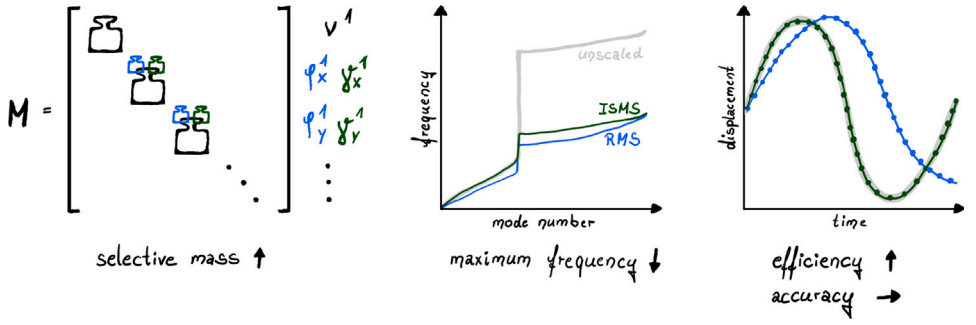

ARTICLE INFO

Keywords:
Hierarchic plate formulations
Selective mass scaling
Frequency spectra
Explicit time integration
Isogeometric analysis
Meshfree discretization

ABSTRACT

The critical time step in explicit time integration methods depends on the highest natural angular frequency of the discretized problem. For shear deformable beam, plate and shell formulations, efficiency is therefore typically limited by the highest transverse shear frequencies, which are mostly of minor importance for the structural response. Direct parametrization using transverse shear variables within hierarchic structural element formulations allows a selective scaling of transverse shear frequencies in a simple manner, while bending frequencies remain practically unaffected. In particular, the novel concept of intrinsically selective mass scaling (ISMS) results in an efficient method that features high accuracy and preserves both linear and angular momentum for both consistent and lumped mass matrices. In addition, ISMS preserves the diagonal structure of lumped mass matrices. Similar to the underlying intrinsically locking-free, hierarchic concept for shear deformable structural element formulations, ISMS retains its beneficial properties for any smooth discretization scheme. In this contribution, we extend recent research on ISMS for beam formulations to the case of shear deformable plate formulations. We test our novel concept with respect to accuracy and efficiency by means of selected numerical experiments. We study both frequency spectra and the transient behavior in explicit time integration. To demonstrate the generality of ISMS, exemplarily both isogeometric

* Corresponding author.
E-mail addresses: krauss@ibb.uni-stuttgart.de (L.-M. Krauß), thierer@ibb.uni-stuttgart.de (R. Thierer), bischoff@ibb.uni-stuttgart.de (M. Bischoff), bastian.oesterle@tuhh.de (B. Oesterle).

https://doi.org/10.1016/j.cma.2024.117430
Received 12 June 2024; Received in revised form 26 September 2024; Accepted 26 September 2024
Available online 8 October 2024

discretizations based on B-splines and meshfree discretizations using local maximum-entropy approximants are investigated.

1. Introduction

Shear deformable structural models like Timoshenko beams, Mindlin plates, and Reissner–Mindlin shells may exhibit superior representation of the real load-bearing behavior in comparison to structural models that neglect transverse shear deformation. This means that not only bending deformation but also transverse shear deformation is taken into account. For structural dynamics, shear deformable models become even more important due to the consideration of rotational inertia in addition to translational inertia. As a consequence, the relevant natural angular frequencies associated with bending modes are represented more accurately than, for instance, in the Euler–Bernoulli beam and the Kirchhoff plate model, and do not reach unphysically high values, as shown in [1] for beam models. At the same time, transverse shear frequencies are included in the frequency spectrum. Depending on the structure's slenderness, they are usually significantly higher than the bending frequencies. Within explicit time integration, this leads to decreasing efficiency, since the critical time step Δt_{crit} directly depends on the highest natural angular frequency of the discretized system $\omega_{\max}$:

$$\Delta t_{\text{crit}} = \frac{2}{\omega_{\max}} . \tag{1}$$

In order to scale down the often unimportant and/or unphysical highest frequencies, while simultaneously preserving important low frequencies, selective mass scaling (SMS) methods were introduced. There exist several approaches for finite element formulations that are based on displacement variables only, see for instance [2,3], among others. Today, conventional mass scaling (CMS) is still used in commercial finite element codes on a daily basis, also in conjunction with shear deformable shell elements using rotational variables and explicit time integration. In the particular case of shear deformable element formulations, it is possible to apply CMS solely to the rotational part of the mass matrix, resulting in rotational mass scaling (RMS), which can be denoted as some sort of semi-selective mass scaling. RMS preserves linear momentum and the diagonal structure of a lumped mass matrix (LMM). However, since the entire rotational inertia is manipulated, also rigid body rotations and the bending modes are severely affected. Thus, the angular momentum is increased and the accuracy of important low bending frequencies is decreased. Origins of RMS for shear deformable element formulations can be traced back to Hughes et al. [4] and Belytschko and Mindle [5]. Back in these days, RMS opened the way for efficient explicit shell transient analysis, which is now the ubiquitous technology in automotive crash analysis and other applications. RMS was an enabling technology for the creation of an industry and is still the state-of-the-art in explicit shell analysis. When CMS is applied to both the rotational part and the translational part of a mass matrix, all frequencies are affected and thus the overall physical behavior is modified.

SMS is more accurate than CMS, but typically does not preserve the diagonal structure of a LMM. Non-diagonal mass matrices are ideally avoided in explicit time integration schemes like the central difference method, since they require the solution of a linear system of equations in each time step. This is one of the main reasons why, in explicit schemes, a LMM is typically preferred over a consistent mass matrix (CMM). Another reason is that LMM results in a higher critical time step size than CMM. The additional costs of SMS resulting from the non-diagonality of the mass matrices do not pay off in all applications. That is, SMS based on non-diagonal mass matrices can, but does not necessarily improve the overall computational efficiency.

In this contribution, we present an intrinsically selective mass scaling (ISMS) approach, which combines the simplicity of CMS and the accuracy of SMS, leading to high overall efficiency. The key to ISMS is its use of hierarchic structural element formulations, which were initially developed for static problems, see for instance [6–8]. Hierarchic formulations are based on reparametrizations of the kinematic equations in order to enable bending deformations without transverse shear, resulting in structural element formulations being intrinsically free from transverse shear locking. In analogy, when inertia is included, the parametrization using distinct transverse shear variables in hierarchic formulations leads to transverse shear inertia. This enables direct and isolated access to transverse shear frequencies, while keeping bending frequencies mostly unaffected. We further enhance previous work on ISMS, presented in Oesterle et al. [9] for hierarchic beam formulations, by several aspects. In particular, we extend the concept of ISMS to plate formulations, we investigate transient analyses, and we study effects of different discretization schemes on the accuracy.

The paper is organized as follows: An overview on various plate formulations for linear dynamics, including mass matrices, is given in Section 2. In Section 3, the concept of ISMS for hierarchic plate formulations is presented and compared to existing mass scaling methods. Next, we present a detailed study of frequency spectra and investigate a transient problem in Section 4. The accuracy of the results in terms of effects resulting from locking, from mass lumping, and from the selective nature of mass scaling is discussed. To demonstrate the generality of ISMS, we compare results from discretizations based on isogeometric analysis (IGA) using B-Splines and based on a meshfree method using maximum-entropy approximants. Finally, our findings are summarized and an outlook on future work is given in Section 5.

2. Shear deformable plate formulations in the context of structural dynamics

2.1. Mindlin plate model

In this contribution, we focus on the shear deformable Mindlin plate model assuming linearized kinematics and linear elastic, isotropic and homogeneous material behavior, as presented in [10]. The kinematic variables and stress resultants are visualized in

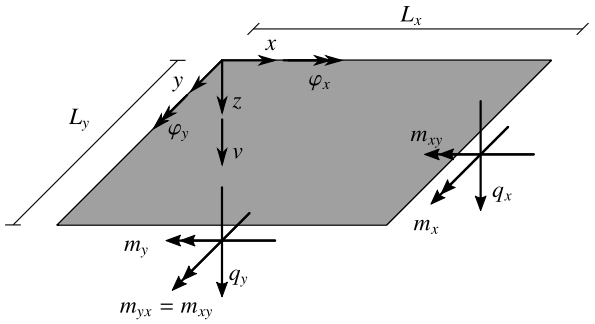

Fig. 1. Kinematic variables and stress resultants (bending moments m_x and m_y, twisting moment m_{xy} and transverse shear forces q_x and q_y) within plate theory.

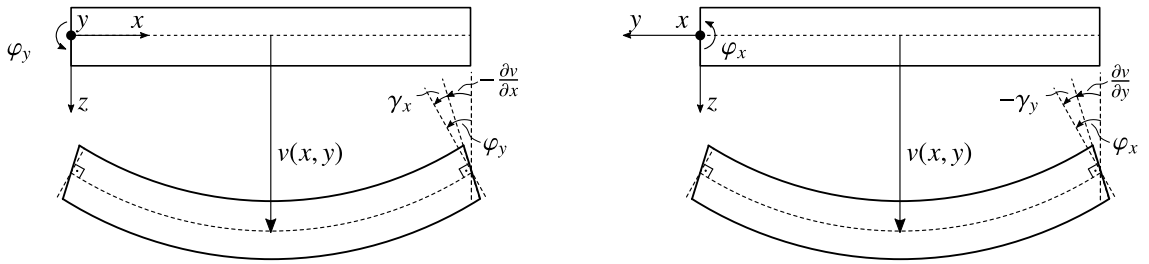

Fig. 2. Linearized kinematics of Mindlin plate model.

Fig. 1. While the transverse shear rotations are assumed to be zero in the Kirchhoff plate model [11], they are taken into account in the Mindlin model, that is: $\gamma_{xz} = \gamma_x \neq 0$ and $\gamma_{yz} = \gamma_y \neq 0$, see Fig. 2. In the Kirchhoff plate model, all kinematic equations can be expressed as a function of the mid-surface displacement only, that is $v(x, y)$. For the Mindlin plate model, two additional kinematic variables are needed to describe transverse shear strain effects. Different choices for these kinematic variables within the parametrization lead to different formulations and are discussed in Section 2.2.

In structural dynamics, taking transverse shear deformation into account becomes even more important than in statics, since shear deformable models allow for a more accurate representation of bending frequencies. While the Kirchhoff model only considers translational inertia, the Mindlin model also includes rotational inertia. As a consequence, the magnitudes of the bending frequencies differ for the two models. Additionally, within the Mindlin model not only bending modes but also transverse shear modes are included. For a deeper insight into the main differences between the Kirchhoff and the Mindlin plate model, we compare frequency spectra of a simply supported square plate. To achieve simple support boundary conditions, we enforce $v = 0$ along all boundaries for both models. For the Mindlin model the additional boundary condition $\varphi_x = 0$ is applied on the edges $x = 0$ and $x = L_x$ as well as $\varphi_y = 0$ on the edges $y = 0$ and $y = L_y$ (hard support boundary condition). The analytical solution for the natural angular frequencies of a rectangular plate according to the Kirchhoff model, see for instance [12,13], are given by

$$\omega_{mn} = \pi^2 \left[\left(\frac{m}{L_x} \right)^2 + \left(\frac{n}{L_y} \right)^2 \right] \sqrt{\frac{D}{\rho d}}, \tag{2}$$

with L_x and L_y denoting the plate's length in x- and y-direction, respectively. Density and plate modulus are denoted as ρ and D, with $D = \frac{Ed^3}{12(1-\nu^2)}$ being a function of Young's modulus E, Poisson's ratio ν and the plate's thickness d. In the continuous case, Eq. (2) results in one bending frequency for every combination of m and n, with $m, n \in \mathbb{N}^+$. The parameters m and n can be interpreted as the numbers of half-waves in each direction for the modes as shown in Fig. 3 for a square plate. On the left, the node lines for which $v(x, y) = 0$ holds are shown for the lowest modes. The diagram on the right illustrates the mode corresponding to $m = n = 3$.

For analytical solutions of the frequency spectrum according to the Mindlin model, we refer to Soedel [13]. The same equations in slightly different notations can be found, for instance, in [14,15]. For the Mindlin model, the shear correction factor κ and the shear modulus $G = \frac{E}{2(1+\nu)}$ are additionally defined. The corresponding natural angular frequencies can be calculated by solving the equation

$$\det \begin{bmatrix} a_{11} - \rho d \omega_{mn}^2 & a_{12} & a_{13} \\ a_{21} & a_{22} - \frac{\rho d^3}{12} \omega_{mn}^2 & a_{23} \\ a_{31} & a_{32} & a_{33} - \frac{\rho d^3}{12} \omega_{mn}^2 \end{bmatrix} = 0, \tag{3}$$

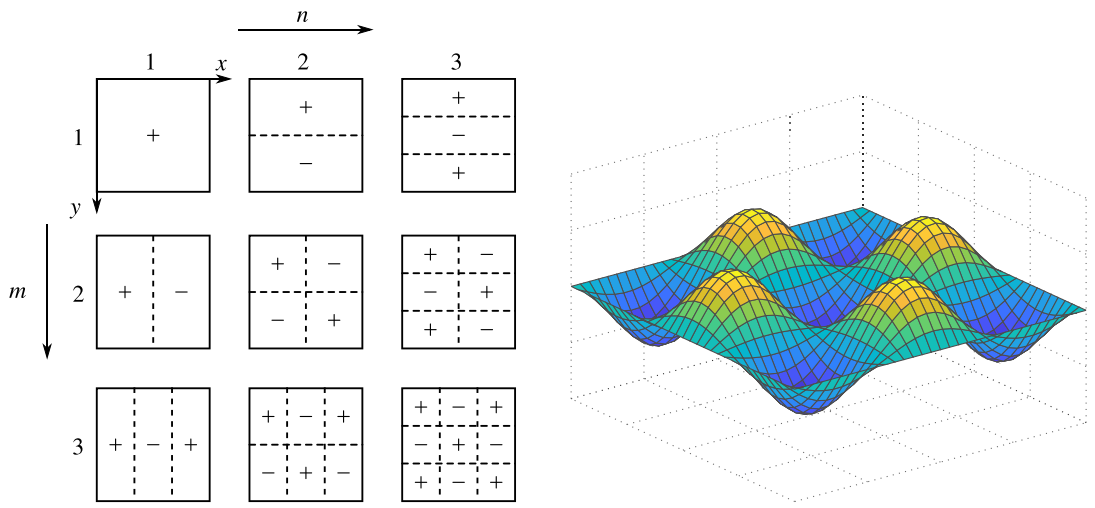

Fig. 3. Left: node lines of bending modes of a square plate, depending on variables m and n according to [13]. Right: visualization of bending mode for $m = 3$ and $n = 3$.

with

$$
\begin{aligned}
a_{11} &= \kappa G d \left[\left(\frac{m\pi}{L_x} \right)^2 + \left(\frac{n\pi}{L_y} \right)^2 \right], & a_{12} &= a_{21} = \kappa G d \frac{m\pi}{L_x}, \\
a_{22} &= D \left[\left(\frac{m\pi}{L_x} \right)^2 + \frac{1-\nu}{2} \left(\frac{n\pi}{L_y} \right)^2 \right] + \kappa G d, & a_{13} &= a_{31} = \kappa G d \frac{n\pi}{L_y}, \\
a_{33} &= D \left[\frac{1-\nu}{2} \left(\frac{m\pi}{L_x} \right)^2 + \left(\frac{n\pi}{L_y} \right)^2 \right] + \kappa G d, & a_{23} &= a_{32} = D \frac{1+\nu}{2} \frac{m\pi}{L_x} \frac{n\pi}{L_y}.
\end{aligned} \tag{4}
$$

Since Eq. (3) is cubic in ω_{mn}^2, each combination of m and n leads to three positive natural angular frequencies, one belonging to a bending mode and the remaining two to transverse shear modes.

Now, we investigate the magnitudes of bending frequencies according to both models. This is done in analogy to Felippa et al. [1], where the bending frequencies of a Bernoulli beam are compared to those of a Timoshenko beam. Fig. 4 shows the dispersion curves $\Omega(k)$ on the left and the phase velocities Ω/k on the right. For all the curves, we assume a square plate with $L = L_x = L_y = 10\,\mathrm{m}$ and thickness $d = 0.1\,\mathrm{m}$. The material properties are chosen as $E = 2.1 \cdot 10^{11}\,\mathrm{N/m^2}$, $\nu = 0.3$, $\kappa = 5/6$ and $\rho = 7800\,\mathrm{kg/m^3}$. Furthermore, to avoid the dependence on two variables m and n, only the curves for $m = n = 1 \ldots 250$ are plotted. The dispersion relation defines the correlation between dimensionless angular frequency $\Omega_m = \frac{L}{c_0}\omega_m$ and dimensionless wavenumber $k_m = 2\pi \frac{L}{\lambda_m}$ with $\lambda_m = \frac{2L}{m}$ being the wavelength and $c_0 = \sqrt{E/\rho}$ the reference phase velocity. Significant differences between both theories can be observed. The dispersion curves are linear for the Mindlin model and quadratic for the Kirchhoff model. As a consequence, in the case of the Kirchhoff plate model, the phase velocities Ω/k assume unphysical, infinitely high values in the limit $k \to \infty$. Constant values for phase velocities are obtained by the Mindlin model, which is a physically sound behavior. The results from Fig. 4 for plate models are qualitatively identical to comparable results obtained from Timoshenko and Bernoulli beams, as can be seen in [1], and highlight the markedly difference between the Mindlin model and the Kirchhoff model in structural dynamics.

2.2. Standard and hierarchic Mindlin plate formulations

The starting point for structural dynamics of shear deformable plates is d'Alembert's principle, which states that the sum of the virtual internal work, the virtual kinetic work, and the virtual external work is equal to zero:

$$\delta W = \delta W_{\mathrm{int}} + \delta W_{\mathrm{kin}} + \delta W_{\mathrm{ext}} = 0\,. \tag{5}$$

In this contribution, we do not take into account damping effects. The internal virtual work is described by

$$\delta W_{\mathrm{int}} = -\int_{\Omega} \underbrace{(\delta \mathbf{u}^{\mathrm{T}} \mathbf{L}^{\mathrm{T}})}_{\delta\boldsymbol{\varepsilon}} \underbrace{\mathbf{C}(\mathbf{L}\mathbf{u})}_{\boldsymbol{\sigma}} \,\mathrm{d}\Omega\,, \tag{6}$$

where the virtual strain components $\delta\boldsymbol{\varepsilon}$ are calculated from the virtual displacements $\delta\mathbf{u}$ and the differential operator $\mathbf{L}$. The stresses are obtained via the material law $\boldsymbol{\sigma} = \mathbf{C}\boldsymbol{\varepsilon} = \mathbf{C}(\mathbf{L}\mathbf{u})$, with $\mathbf{C}$ being the material matrix. The virtual kinetic work includes the density

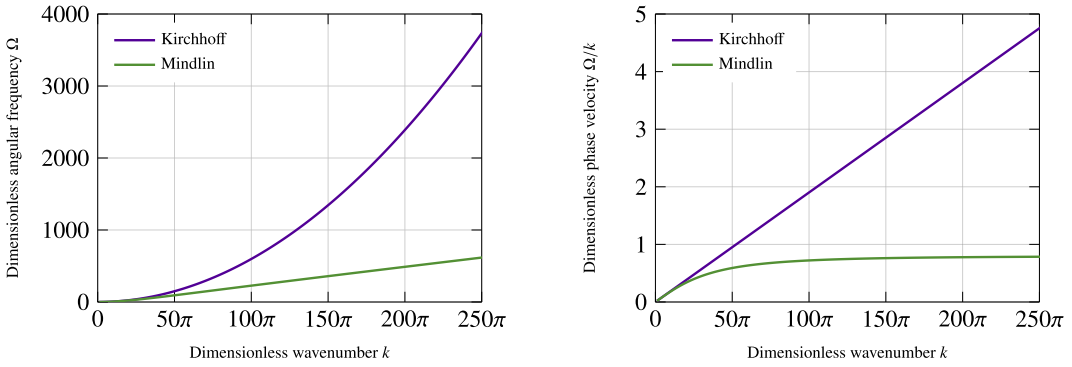

Fig. 4. Spectral behavior of a continuous square plate with $\nu = 0.3$ and $m = n$ for the Kirchhoff model and bending branch for the Mindlin model. Left: dispersion curves $\Omega(k)$. Right: phase velocities Ω/k.

matrix $\boldsymbol{\rho}$ and the acceleration $\ddot{\mathbf{u}}$:

$$\delta W_{\text{kin}} = -\int_{\Omega} \delta\mathbf{u}^{\mathrm{T}} \boldsymbol{\rho} \ddot{\mathbf{u}} \, \mathrm{d}\Omega \,. \tag{7}$$

The virtual external work consists of a term due to external volume loads $\mathbf{b}$ and surface tractions $\hat{\mathbf{t}}$:

$$\delta W_{\text{ext}} = \int_{\Omega} \delta\mathbf{u}^{\mathrm{T}} \mathbf{b} \, \mathrm{d}\Omega + \int_{\Gamma_\sigma} \delta\mathbf{u}^{\mathrm{T}} \hat{\mathbf{t}} \, \mathrm{d}\Gamma \,. \tag{8}$$

For the discretized problem, the matrix of shape functions $\mathbf{N}$ and the strain–displacement operator $\mathbf{B} = \mathbf{NL}$ are introduced, resulting in the approximations

$$\begin{aligned} \mathbf{u} &\approx \mathbf{u}_{\text{h}} = \mathbf{N}\mathbf{d} \,, \\ \boldsymbol{\varepsilon} &\approx \boldsymbol{\varepsilon}_{\text{h}} = \mathbf{LN}\mathbf{d} =: \mathbf{B}\mathbf{d} \end{aligned} \tag{9}$$

for the displacements $\mathbf{u}$ and strains $\boldsymbol{\varepsilon}$. This also applies to the virtual variables

$$\begin{aligned} \delta\mathbf{u} &= \mathbf{N}\delta\mathbf{d} \,, \\ \delta\boldsymbol{\varepsilon} &= \mathbf{B}\delta\mathbf{d} \,. \end{aligned} \tag{10}$$

Inserting Eqs. (6) to (10) into Eq. (5) yields the discretized form of d'Alembert's principle

$$\begin{aligned} &\sum_{e=1}^{n_{ele}} \int_{\Omega_{ele}} \delta\mathbf{d}^{\mathrm{T}} \underbrace{\mathbf{B}^{\mathrm{T}}\mathbf{C}\mathbf{B}}_{\mathbf{k}^e} \mathbf{d} \, \mathrm{d}\Omega + \sum_{e=1}^{n_{ele}} \int_{\Omega_{ele}} \delta\mathbf{d}^{\mathrm{T}} \underbrace{\mathbf{N}^{\mathrm{T}}\boldsymbol{\rho}\mathbf{N}}_{\mathbf{m}^e} \ddot{\mathbf{d}} \, \mathrm{d}\Omega \\ &= \sum_{e=1}^{n_{ele}} \delta\mathbf{d}^{\mathrm{T}} \underbrace{\left(\int_{\Omega_{ele}} \mathbf{N}^{\mathrm{T}}\mathbf{b} \, \mathrm{d}\Omega + \int_{\Gamma_\sigma} \mathbf{N}^{\mathrm{T}}\hat{\mathbf{t}} \, \mathrm{d}\Gamma \right)}_{\mathbf{f}^e}, \text{ where } \delta\mathbf{d} = 0 \text{ on } \Gamma_u \,. \end{aligned} \tag{11}$$

Up to this point, the introduced equations are not restricted to a particular structural model or discretization scheme. In the following, we specify the operators and variables according to the Mindlin plate model. The material law connects the stress resultants from Fig. 1 to the strain components from Fig. 2 via the material matrix $\mathbf{C}$

$$\underbrace{\begin{bmatrix} q_x \\ q_y \\ m_x \\ m_y \\ m_{xy} \end{bmatrix}}_{\boldsymbol{\sigma}} = \underbrace{\begin{bmatrix} \kappa Gd & 0 & 0 & 0 & 0 \\ 0 & \kappa Gd & 0 & 0 & 0 \\ 0 & 0 & D & \nu D & 0 \\ 0 & 0 & \nu D & D & 0 \\ 0 & 0 & 0 & 0 & \frac{D}{2}(1-\nu) \end{bmatrix}}_{\mathbf{C}} \underbrace{\begin{bmatrix} \gamma_x \\ \gamma_y \\ \kappa_x \\ \kappa_y \\ 2\kappa_{xy} \end{bmatrix}}_{\boldsymbol{\varepsilon}} . \tag{12}$$

The consistent element mass matrix $\mathbf{m}_{\text{C}}$ is constructed by the density matrix $\boldsymbol{\rho}$, which is independent of the choice of primary variables, and the matrix of shape functions w.r.t. the displacement v and the total rotations φ_x and φ_y, which is introduced as $\mathbf{N}_{\text{m}}$:

$$\mathbf{m}_{\text{C}} = \int_{\Omega_{ele}} {\mathbf{N}_{\text{m}}}^{\mathrm{T}} \boldsymbol{\rho} \mathbf{N}_{\text{m}} \, \mathrm{d}\Omega \tag{13}$$

Table 1
Overview of the kinematic equations of various Mindlin plate formulations with different parametrizations (M-st, M-hr, M-hd).

Formulation	Displacement	Total rotations	Shear strains	Curvature
M-st	v	$\varphi_x = \varphi_x$	$\gamma_x = \frac{\partial v}{\partial x} + \varphi_y$	$\kappa_x = \frac{\partial \varphi_y}{\partial x}$
		$\varphi_y = \varphi_y$	$\gamma_y = \frac{\partial v}{\partial y} - \varphi_x$	$\kappa_y = -\frac{\partial \varphi_x}{\partial y}$
				$\kappa_{xy} = \frac{1}{2}\left(\frac{\partial \varphi_y}{\partial y} - \frac{\partial \varphi_x}{\partial x}\right)$
M-hr	v	$\varphi_x = \frac{\partial v}{\partial y} - \gamma_y$	$\gamma_x = \gamma_x$	$\kappa_x = -\frac{\partial^2 v}{\partial x^2} + \frac{\partial \gamma_x}{\partial x}$
		$\varphi_y = -\frac{\partial v}{\partial x} + \gamma_x$	$\gamma_y = \gamma_y$	$\kappa_y = -\frac{\partial^2 v}{\partial y^2} + \frac{\partial \gamma_y}{\partial y}$
				$\kappa_{xy} = -\frac{\partial^2 v}{\partial x \partial y} + \frac{1}{2}\left(\frac{\partial \gamma_x}{\partial y} + \frac{\partial \gamma_y}{\partial x}\right)$
M-hd	v	$\varphi_x = \frac{\partial (v - v_{s_y})}{\partial y}$	$\gamma_x = \frac{\partial v_{s_x}}{\partial x}$	$\kappa_x = -\frac{\partial^2 v}{\partial x^2} + \frac{\partial^2 v_{s_x}}{\partial x^2}$
		$\varphi_y = -\frac{\partial (v - v_{s_x})}{\partial x}$	$\gamma_y = \frac{\partial v_{s_y}}{\partial y}$	$\kappa_y = -\frac{\partial^2 v}{\partial y^2} + \frac{\partial^2 v_{s_y}}{\partial y^2}$
				$\kappa_{xy} = -\frac{\partial^2 v}{\partial x \partial y} + \frac{1}{2}\left(\frac{\partial^2 v_{s_x}}{\partial x \partial y} + \frac{\partial^2 v_{s_y}}{\partial x \partial y}\right)$

with

$$\boldsymbol{\rho} = \begin{bmatrix} \rho d & 0 & 0 \\ 0 & \frac{\rho d^3}{12} & 0 \\ 0 & 0 & \frac{\rho d^3}{12} \end{bmatrix}. \tag{14}$$

The matrix $\mathbf{N}_{\mathrm{m}}$ depends on the choice of primary variables and the corresponding plate formulations used in this contribution are

- **M-st**: standard (st) Mindlin (M) plate formulation using the total displacement v and the total rotations φ_x and φ_y as primary variables,
- **M-hr**: Mindlin plate formulation with hierarchic rotations (hr) using the total displacement v and the transverse shear rotations γ_x and γ_y as primary variables, see [6],
- **M-hd**: Mindlin plate formulation with hierarchic displacements (hd) using the total displacement v and the transverse shear displacements v_{s_x} and v_{s_x} as primary variables, see [16].

The differential operator $\mathbf{L}$ for the three different plate formulations can be derived from the kinematic equations in Table 1. For both hierarchic formulations, C^1-continuity for the shape functions is required, since the variational indices of the corresponding weak forms are two. This requirement can be fulfilled by different discretization schemes such as isogeometric analysis based on NURBS or meshfree methods based on maximum-entropy approximants.

Since the formulations M-hr and M-hd include the Kirchhoff plate formulation as a basis for vanishing transverse shear deformation, that is $\gamma_x = \gamma_y = 0$ or $v_{s_x} = v_{s_y} = 0$, respectively, they are called *hierarchic*, see [6,7]. While the standard formulation M-st suffers from transverse shear locking, both hierarchic formulations are intrinsically free from transverse shear locking, that is, they intrinsically avoid transverse shear locking on the level of theory, independent of the particular discretization scheme, see [6–8,17,18]. Transverse shear locking is visible in the form of an imbalance in the corresponding kinematic equations of the M-st formulation

$$\gamma_x = \frac{\partial v}{\partial x} + \varphi_y \qquad \text{and} \qquad \gamma_y = \frac{\partial v}{\partial y} - \varphi_x\,, \tag{15}$$

which leads to parasitic transverse shear strains for any equal order interpolation of the primary variables. For the M-hr formulation, the imbalance is shifted from the transverse shear strains to the curvature. In the static case, no significant influence on the results for displacements and stresses (see [7,8,16]) has been observed, but, in the dynamic case, this imbalance has a more significant influence on the bending frequencies for very thick plates. Therefore, this phenomenon is named *bending locking*, but not considered further within this study, since we do not treat examples with very thick plates. In Batoz et al. [19], a closely related bending locking effect has been observed for mixed plate finite element formulations based on a modified Hellinger–Reissner principle. For the M-hd formulation, the kinematic equations are perfectly balanced. Thus, locking effects occur neither in static nor in dynamic analyses, and, therefore, M-hd is fully locking-free. To overcome the imbalances in the kinematic equations for the M-st and the M-hr formulation, one possibility is to choose shape functions for the rotations one order lower than those for the displacements. In the context of isogeometric Mindlin plates, this concept has been introduced in Beirão da Veiga et al. [20]. Using non-equal order interpolation instead of equal order interpolation is only possible for discretization schemes using polynomial-based shape functions. Within the present contribution, in the case of non-equal order interpolation we add the abbreviation *low* to the used plate formulation. The resulting elements **M-st-low** and **M-hr-low** are fully locking-free. Whenever their numerical results are practically identical, we refer to them as **M-low**.

2.3. Consistent and lumped mass matrices

Consistent element mass matrices $\mathbf{m}_{\mathrm{C}}$ can be computed from Eq. (13) and assembled to the global CMM. They are symmetric but non-diagonal, just as element stiffness matrices. However, since non-diagonal mass matrices lead to decreasing efficiency in

explicit time integration algorithms, mass schemes are typically used to construct diagonal mass matrices and, thus, to increase efficiency. The simplest and most commonly used procedure is row-sum lumping. The accuracy of row-sum lumping depends on the discretization scheme. Within an isogeometric discretization, the LMM constructed by row-sum lumping is only second order accurate, independent of the polynomial degrees of the shape functions [21]. There are many other methods to construct diagonal mass matrices, but most of them are only well suited for a certain discretization scheme or for elements with displacement degrees of freedom only. For instance, HRZ lumping [22] (named after the authors) is not well suited for finite elements with rotational degrees of freedom [1]. According to Archer and Whalen [23], shear deformable elements may produce inaccurate results when LMMs are used. The development of accurate and efficient mass lumping schemes, in particular for smooth discretization schemes like IGA, is an important current research topic, as can be seen from [24–29], among others. However, so far, row-sum lumping is still state of the art in IGA and is used within the present contribution. Here, we focus on a novel mass *scaling* method and not on a particular mass *lumping* scheme. But the novel mass scaling method presented herein is applicable to any smooth, at least C^1-continuous, discretization scheme, independent of the mass lumping technique and, thus, extensions to novel lumped mass matrices is expected to work out in a straight-forward manner.

3. Intrinsically selective mass scaling

3.1. General concept

Due to its simplicity, CMS is routinely used in commercial explicit finite element codes. It can be used for all types of elements based on both displacement and rotational degrees of freedom, as can be seen for instance in [30]. CMS preserves the diagonal structure of the LMM, but modifies all frequencies. Thus, CMS can severely change the dynamic response of the discretized system, coming along with a loss of accuracy. In the specific case of Reissner–Mindlin shell elements, it is possible to apply CMS solely to the rotational part of the mass matrix, which results in preservation of both linear momentum and the diagonal structure of a LMM, see for instance [4,5]. However, this RMS concept affects the entire rotational inertia, coming along with a modification of rigid body rotations, angular momentum and bending frequencies. In fact, RMS is used by default for the construction of the LMM of the isogeometric Reissner–Mindlin shell element proposed by Benson et al. [31] and used within *LS-DYNA* in [32]. Therein, the amount of scaling is chosen in such a way that rotational inertia does not limit the critical time step.

In contrast to CMS, SMS aims at selectively scaling the high frequencies while preserving important low frequency contents. In the context of discretization methods, the highest frequencies are always physically not meaningful, regardless of the structural model, because they represent artificial “mesh modes”. By this concept, SMS is more accurate than CMS, but it typically does not preserve the diagonal structure of a LMM. Non-diagonal mass matrices negatively affect the efficiency of explicit time integration schemes, since a linear system of equations has to be solved in each time step. Thus, SMS methods based on non-diagonal mass matrices do not necessarily increase the overall computational efficiency. Nevertheless, the SMS method presented in Olovsson et al. [2] is state-of-the-art in commercial software like *LS-DYNA* and *RADIOSS* [3] and its use can pay off for certain problem classes. But, when used along with elements possessing rotational degrees of freedom, for instance Reissner–Mindlin shell elements, SMS inspired from [2] cannot scale down the highest frequency, as shown in [33]. In the particular case of shear deformable shell elements with rotational degrees of freedom, typically SMS is solely used for the modification of the translational part of the mass matrix, while the rotational part still has to be modified by RMS.

The concept of ISMS, first presented in Oesterle et al. [9], combines the advantages of both CMS and SMS. ISMS is as simple as CMS, preserves the diagonality of LMMs and is as effective as a SMS scheme. ISMS takes advantage of hierarchic formulations and their parametrizations using distinct transverse shear primary variables, which are the main source of ISMS’ intrinsically selective nature. For the M-hr plate formulation, these are the transverse shear rotations γ_x and γ_y. For the M-hd plate formulation, generalized transverse shear displacements v_{s_x} and v_{s_y} are introduced. As a consequence, transverse shear inertia can be directly accessed and, therefore, transverse shear frequencies can be selectively scaled without a significant change of the bending frequencies. Since ISMS is based on the hierarchic concept, it similarly retains its fundamental properties for any smooth discretization scheme. Like CMS and RMS, ISMS is a local mass scaling scheme, that is, ISMS can be applied on local or element level followed by subsequent assembly of the system mass matrix. In the following, ISMS is described on element level, whereby application on the global level is straightforward and leads to identical results.

In the following, ISMS is described on element level, whereby application on the global level is straightforward. Furthermore, the ISMS scheme can be formulated for both a diagonal LMM and a CMM. The application to both types of mass matrices is shown here to demonstrate ISMS’ effectiveness and selectivity, independent of the used type of mass matrix, in Section 4.3 below.

The scaled CMM $\mathbf{m}_{\mathrm{C}}^{\circ}$ can be described by a Hadamard product (entry-wise product) of the scaling matrix $\boldsymbol{\alpha}_{\mathrm{C}}$ and the unscaled CMM $\mathbf{m}_{\mathrm{C}}$, while ISMS of the LMM $\mathbf{m}_{\mathrm{L}}$ is performed in similar fashion:

$$\mathbf{m}_{\mathrm{C}}^{\circ} = \boldsymbol{\alpha}_{\mathrm{C}} \odot \mathbf{m}_{\mathrm{C}} \,, \tag{16}$$

$$\mathbf{m}_{\mathrm{L}}^{\circ} = \boldsymbol{\alpha}_{\mathrm{L}} \odot \mathbf{m}_{\mathrm{L}} \,. \tag{17}$$

The corresponding scaling matrices read

$$\boldsymbol{\alpha}_{\mathrm{C}} = \begin{bmatrix} \boldsymbol{\alpha}_{\mathrm{C},3\times3} & \cdots & \boldsymbol{\alpha}_{\mathrm{C},3\times3} \\ \vdots & \ddots & \vdots \\ \boldsymbol{\alpha}_{\mathrm{C},3\times3} & \cdots & \boldsymbol{\alpha}_{\mathrm{C},3\times3} \end{bmatrix} \qquad \text{with} \qquad \boldsymbol{\alpha}_{\mathrm{C},3\times3} = \begin{bmatrix} 1 & 1 & 1 \\ 1 & \alpha & \alpha \\ 1 & \alpha & \alpha \end{bmatrix}, \tag{18}$$

$$\boldsymbol{\alpha}_{\mathrm{L}} = \begin{bmatrix} \boldsymbol{\alpha}_{\mathrm{L},3\times3} & \mathbf{0}_{3\times3} & \cdots & \mathbf{0}_{3\times3} \\ \mathbf{0}_{3\times3} & \ddots & \ddots & \vdots \\ \vdots & \ddots & \ddots & \mathbf{0}_{3\times3} \\ \mathbf{0}_{3\times3} & \cdots & \mathbf{0}_{3\times3} & \boldsymbol{\alpha}_{\mathrm{L},3\times3} \end{bmatrix} \quad \text{with} \quad \boldsymbol{\alpha}_{\mathrm{L},3\times3} = \begin{bmatrix} 1 & 0 & 0 \\ 0 & \alpha & 0 \\ 0 & 0 & \alpha \end{bmatrix}. \tag{19}$$

A selective reduction of the transverse shear frequencies is achieved for a scaling parameter $\alpha > 1$. The structure of the scaling matrices from Eqs. (18) and (19) assumes an ordering of the element degrees of freedom of the form

$$\mathbf{d} = \left[v^1 \; \gamma_x^1 \; \gamma_y^1 \; \ldots \; v^{n_\mathrm{n}} \; \gamma_x^{n_\mathrm{n}} \; \gamma_y^{n_\mathrm{n}} \right]^{\mathrm{T}}, \tag{20}$$

with n_n being the number of nodes per element. As can be deduced from Eqs. (18) and (19), the scaling parameter α solely acts on the entries related to transverse shear degrees of freedom. More precisely, for $\alpha > 1$, ISMS solely increases the transverse shear part of the total rotational mass, while the translational mass remains unaffected. As a consequence, ISMS naturally preserves both linear and angular momentum. Since ISMS intrinsically selects the part of the inertia related to transverse shear rotation, it allows for scaling of the transverse shear frequencies in a highly selective fashion, that is, bending frequencies remain mostly unaffected by ISMS, coming along with high accuracy in most cases. In addition, as can be deduced from Eq. (19), ISMS preserves the diagonal structure of a LMM, making it as simple as a CMS method.

Beyond this, ISMS is closely related to the above described RMS. In fact, the application of the scaling scheme from Eqs. (16) and (17) to the standard M-st plate formulation results in RMS. While ISMS only affects the shear-related part of the rotational mass, RMS increases the total rotational mass and, thus, RMS does not preserve angular momentum. Furthermore, bending frequencies may be significantly modified by RMS, coming along with reduced accuracy compared to ISMS, which is demonstrated in Section 4.3.

In the present contribution, ISMS is considered solely in conjunction with the M-hr formulation. For the M-hd formulation, practical problems during mass lumping show up. That is, for the M-hd formulation, row-sum lumping leads to a singular LMM. This phenomenon is related to the perfectly balanced kinematic equations, as can be seen in Table 1. This property holds true for any discretization scheme and has already been observed for the shear deformable beam formulation with hierarchic displacements in [9]. This issue could be resolved with other lumping techniques such as HRZ lumping [22]. However, since HRZ lumping is not suitable for meshfree discretizations, we do not use this alternative lumping method in our contribution. Therefore, the M-hd formulation is not further considered within the present study, although ISMS could be directly applied to a CMM rather than to a LMM which is obtained with row-sum lumping.

3.2. Choice of the mass scaling parameter α

So far, it was not discussed how the mass scaling parameter α can be chosen for achieving a reduction of the highest frequency by a certain amount or percentage. In the present study, which is restricted to linear plate dynamics, we follow a simple procedure for defining the scaling parameter α, which is explained in the following. As is shown in Section 4.3, ISMS is highly selective. That is, ISMS is capable of effectively scaling the high shear frequencies, while the bending branch remains mainly unaffected by ISMS. However, assuming no modification of the bending branch means that the maximum reduction of the highest frequency is limited by the highest bending frequency of the discrete spectrum. The highest natural angular bending frequency, that is the target natural angular frequency ω_{ISMS}, can be estimated by the analytical solution or by a discrete spectrum of a discretization with Kirchhoff elements. Inspired by the formula for a single degree of freedom oscillator, the ratio of the scaled to the unscaled maximum natural angular frequency can be estimated by

$$\frac{\omega_{\mathrm{ISMS}}}{\omega_{\max}} \approx \frac{\sqrt{\frac{K}{\alpha M}}}{\sqrt{\frac{K}{M}}} = \sqrt{\frac{1}{\alpha}}. \tag{21}$$

Accordingly, for a known or desired ratio of scaled to unscaled maximum natural angular frequency, the scaling parameter α can be estimated by

$$\alpha \approx \left(\frac{\omega_{\max}}{\omega_{\mathrm{ISMS}}} \right)^2. \tag{22}$$

For a practical application of ISMS, the choice of optimal mass scaling parameters α and efficient and accurate estimates of the allowed critical time step size Δt_{crit} are crucial. This is particularly important in conjunction with the extension of ISMS to nonlinear hierarchic shells formulations, which is planned in future research. In the case of standard, non-hierarchic Reissner–Mindlin shell formulations, α is typically chosen in such a way that rotational inertia does not limit the critical time step. That is, the maximum shear frequency is scaled down to the level of highest membrane frequency. As a consequence, the critical time step Δt_{crit} is then independent of the shell's thickness and typically estimated by geometry-based time step estimators taking into account the in-plane geometry of the shell elements. For further insight we refer to Benson [34], among others.

4. Numerical studies

4.1. Overview

In this section, we investigate the problem of a simply supported square plate in order to study accuracy and efficiency of the introduced ISMS concept in the context of hierarchic plate formulations. The problem setup is shown in Fig. 5 (left), while the

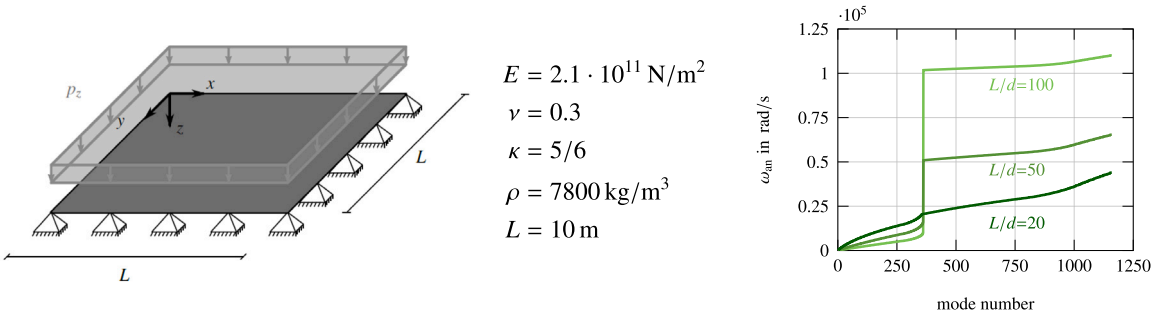

Fig. 5. Left: numerical example of square plate under uniform loading. Middle: geometry and material data. Right: analytical frequency spectra according to the Mindlin plate model in dependence of the slenderness ratio L/d.

geometry and material data are given in Fig. 5 (middle). For the frequency spectra in Sections 4.2 and 4.3 we study a square plate with hard simple support to ensure the comparability with the analytical solution in Section 2.1. For the transient analysis in Section 4.4 only the displacements are fixed on the boundaries (soft support).

Since hierarchic formulations require at least C^1-continuous shape functions, we employ two different smooth discretization schemes, that is, an isogeometric discretization based on quadratic, C^1-continuous B-splines and a meshfree discretization based on maximum-entropy approximants. For isogeometric discretizations, we use quadratic B-splines constructed from an open knot vector. In the case of plate formulations with non-equal order interpolation, that is M-st-low or M-hr-low, we discretize the (transverse shear) rotation field using linear B-splines, that is linear Lagrange polynomials, with the same number of elements as the quadratic B-spline space. For further details on IGA we refer to [35,36]. The basis functions for a meshfree discretization with maximum-entropy approximants are rational exponential functions depending on a parameter $\gamma \in [0, +\infty)$, which defines the locality of the shape functions, see [37]. An introduction to maximum-entropy approximants can be found in [37,38]. For both discretization schemes and for equal order interpolations, a discretization with 21×21 nodes is used, which results in $n_{\mathrm{dof}} = 21 \times 21 \times 3 = 1323$ degrees of freedom for M-st and M-hr. After enforcing Dirichlet boundary conditions $v = 0$ on all four edges Γ_u, the number of unknowns reduces by 80 to 1243 degrees of freedom. To realize a hard support, the boundary condition $\varphi_x = 0$ is applied on the edges $x = 0$ and $x = L_x$ as well as $\varphi_y = 0$ on the edges $y = 0$ and $y = L_y$, reducing the degrees of freedom by 84 to 1159. The corresponding frequency spectra show 361 bending frequencies and 798 transverse shear frequencies. Using non-equal order interpolation, the number of unknowns reduces by enforcing Dirichlet boundary conditions to 1121 degrees of freedom, resulting in 361 bending and 760 transverse shear frequencies for M-st-low and M-hr-low.

The analytical solution for the natural angular frequencies has been introduced in Section 2.1 and serves as a reference in the first part. For this purpose, analytical frequency spectra have been compiled for different slenderness values L/d according to Eqs. (3) and (4). These results are shown in Fig. 5 (right), where L and d represent the plate's side length and thickness, respectively. For comparability with the numerical solutions, 361 analytical bending frequencies using $n, m \in \{1, \ldots, 19\}$ and 798 analytical shear frequencies using $n, m \in \{1, \ldots, 21\}$ are calculated. The 361 analytical bending frequencies and the lowest 760 analytical shear frequencies are considered for comparison with numerical results computed with non-equal order interpolation.

In total, we compare the results obtained from several Mindlin plate formulations, that is **M-st**, **M-hr**, **M-st-low** and **M-hr-low** for three different problem classes. In Section 4.2, we compare the unscaled frequency spectra using **CMM** and **LMM** for both an **isogeometric** and a **meshfree** discretization for both the M-st and the M-hr plate formulations. The M-st-low and M-hr-low plate formulations are studied solely for the isogeometric discretization, since maximum-entropy approximants are not based on polynomials and lower order spaces cannot be constructed in a straight-forward manner. On the basis of the unscaled spectra, in Section 4.3, we study scaled frequency spectra after employing mass scaling for different plate formulations. Here, we study the intrinsically *selective* nature of **ISMS** and compare it to **RMS**. In the third example, see Section 4.4, we investigate the effects of ISMS on accuracy and efficiency of transient analyses employing explicit time integration.

The use of two different discretization schemes and two different types of mass matrices aims at validating that ISMS is indeed an *intrinsically* selective mass scaling scheme, that is, the general effectiveness and accuracy of ISMS is independent of the discretization scheme and the employed type of mass matrix.

4.2. Frequency spectra without mass scaling

First, we compare the spectral accuracy of different shear deformable plate formulations and different mass matrices. We choose a slenderness ratio of $L/d = 100$, for which the bending frequencies and the transverse shear frequencies are clearly separated, as shown in Fig. 5 (right). Fig. 6 shows the ratios of numerical frequencies to analytical frequencies for an isogeometric discretization and for both CMM and LMM.

For all plate formulations, CMM overestimates the first 361 frequencies of the bending branch, while the transverse shear branch is captured very accurately. For M-st, transverse shear locking severely reduces the accuracy in the bending branch. By proper choice of a lower order ansatz for the rotation, M-st-low removes transverse shear locking and thus provides more accurate bending

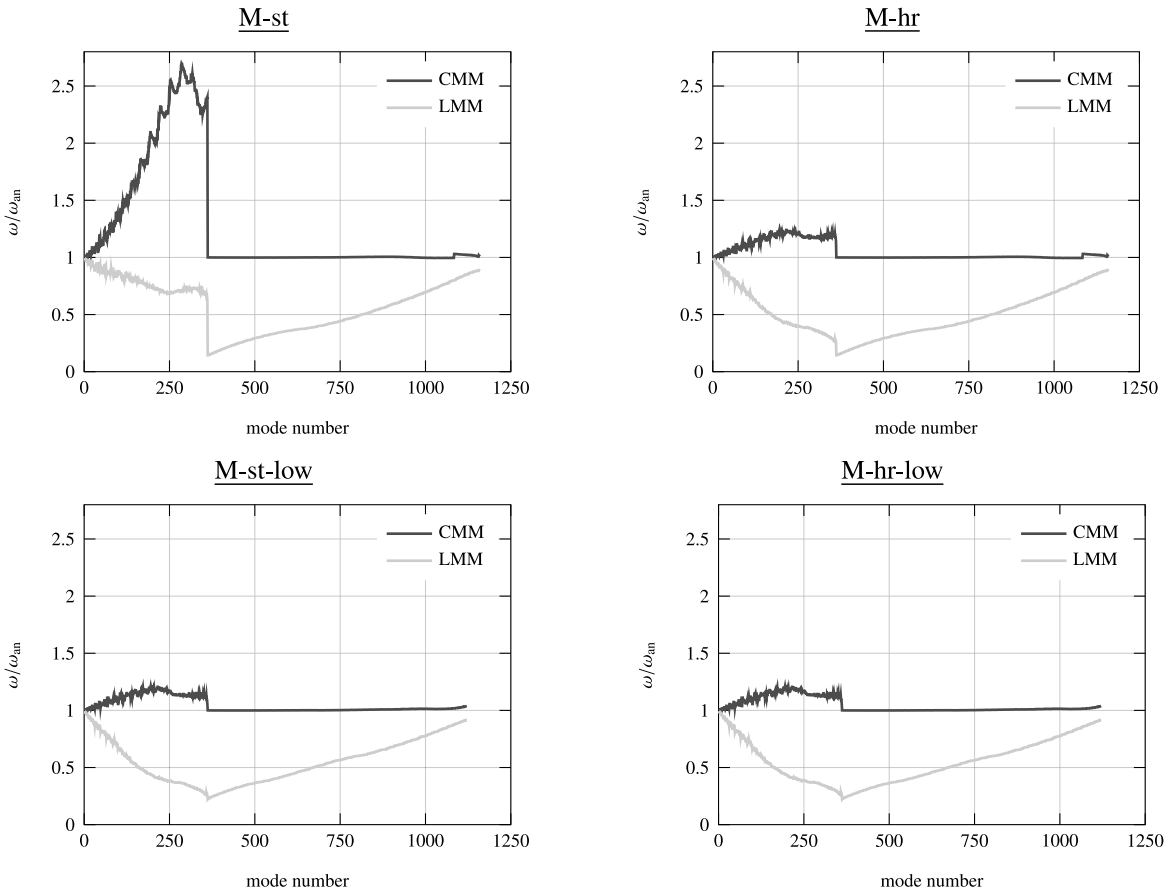

Fig. 6. Ratio of numerical natural angular frequencies ω to analytical natural angular frequencies ω_{an} for slenderness $L/d = 100$ and an **isogeometric** discretization using either **CMM** or **LMM** for **M-st**, **M-hr**, **M-st-low** and **M-hr-low**.

frequencies. A similar observation can be made for M-hr-low, since the results for M-st-low and M-hr-low are practically identical. Also, M-hr shows very good, but slightly less accurate results compared to M-st-low and M-hr-low. This seems to be a consequence of the previously explained bending locking, which is not very pronounced for the chosen slenderness ratio. Outlier frequencies often occur at the end of the spectrum when using isogeometric discretizations. In our numerical example they are hardly noticeable due to the visualization of relative values ω/ω_{an}. On top of that, the low polynomial degree $p = 2$ does not cause significant outlier frequencies in our example. For increasing polynomial degrees, outlier frequencies are pronounced, as shown in [21]. We study the effect of outlier frequencies on ISMS in Section 4.3.

As expected, the accuracy of numerical frequency spectra computed using a row-sum LMM is lower for all plate formulations. Here, all numerical frequencies underestimate the analytical ones. Surprisingly, the highest accuracy within the bending branch is obtained by the M-st formulation. Actually, this is only due to two opposing, negative effects coincidentally canceling. Lumping pushes the bending branch down, while transverse shear locking results in overstiff bending frequencies and shifts the bending branch up again. This unexpected allegedly positive effect of transverse shear locking vanishes for the locking-free M-st-low formulation. The frequency spectra for both locking-free formulations M-st-low and M-hr-low are again practically identical. Thus, they build the perfect basis for further studies on mass scaling, as demonstrated in the next subsection.

Before, however, the accuracy of frequency spectra obtained by the meshfree discretization is investigated. For the meshfree discretization within this study there is no locking-free formulation, but the frequency spectra of M-st and M-hr can be compared to those obtained by the isogeometric discretization. The parameter γ, which controls the support of maximum-entropy approximants, influences the accuracy. Thus, Fig. 7 shows the frequency spectra for two different values of γ, that is $\gamma = 1.2$ and $\gamma = 1.6$, using CMM as well as a LMM obtained by row-sum lumping. Similar conclusions as for the spectra obtained using isogeometric discretization can be drawn. The negative effect of transverse shear locking is clearly visible in the bending branch for M-st with CMM, while the M-hr formulation is more accurate for CMM. As for the isogeometric discretization, a row-sum LMM is overall less accurate than a CMM. We choose $\gamma = 1.2$ for the subsequent studies, since the results for CMM as well as results of a static analysis (not shown) are slightly more accurate than for $\gamma = 1.6$.

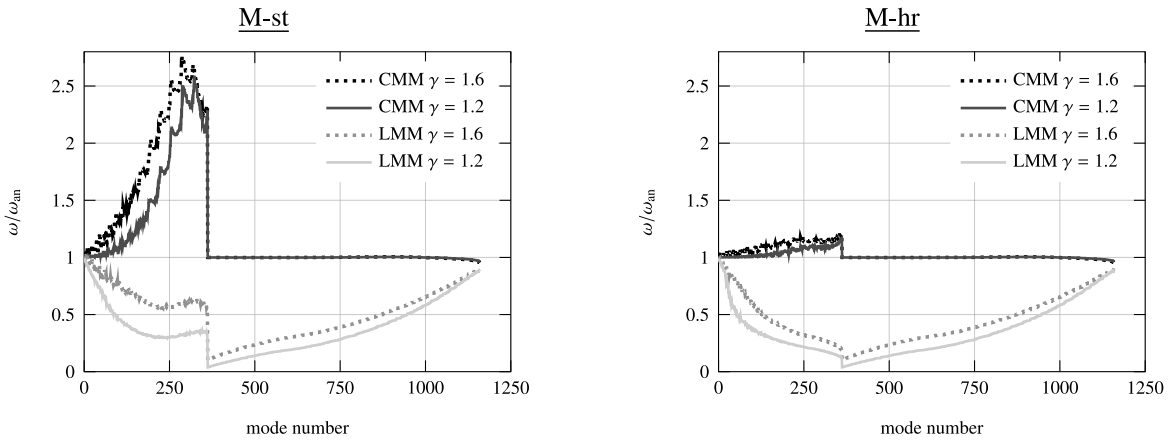

Fig. 7. Ratio of numerical natural angular frequencies ω to analytical natural angular frequencies ω_{an} for slenderness $L/d = 100$ and a **meshfree** discretization with $\gamma = 1.2$ and $\gamma = 1.6$ using either **CMM** or **LMM** for **M-st** and **M-hr**.

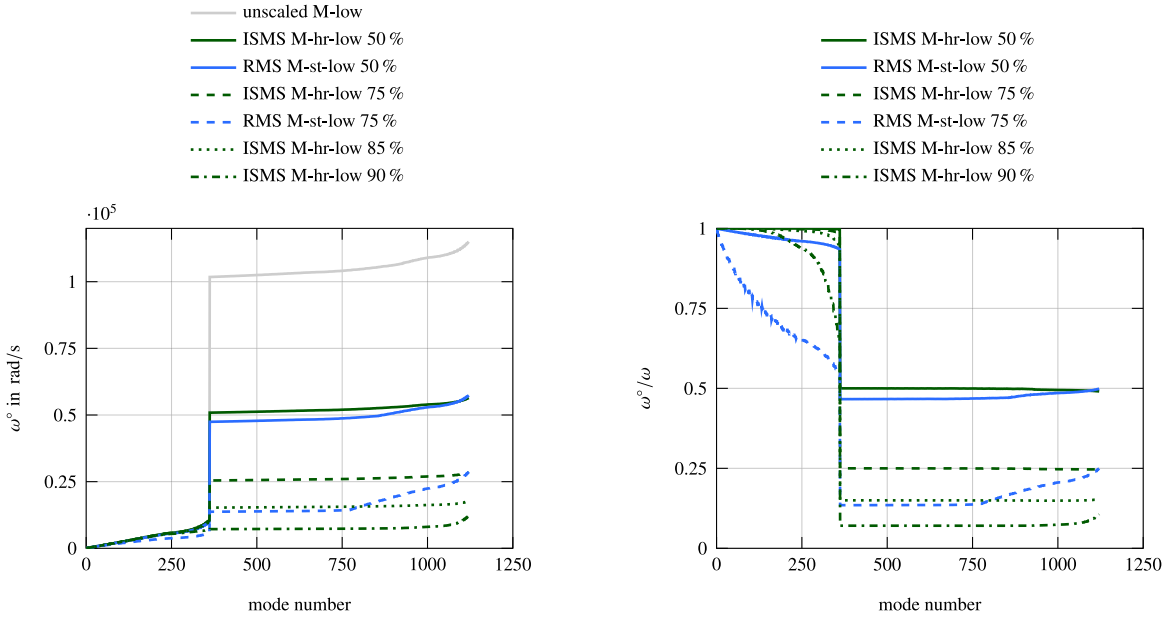

Fig. 8. Frequency spectra for **M-st-low** with **RMS** and for **M-hr-low** with **ISMS** with **isogeometric** discretization for different levels of scaling using **CMM** and slenderness $L/d = 100$. Left: absolute values of natural angular frequencies ω°. Right: ratio of scaled to unscaled natural angular frequencies ω°/ω.

4.3. Frequency spectra with mass scaling

In this subsection, we study the intrinsically selective nature of ISMS and compare it to RMS for the plate problem shown in Fig. 5 and a slenderness ratio of $L/d = 100$. In a first step, we focus on the fully locking-free formulations M-st-low and M-hr-low using CMM and an isogeometric discretization. The two formulations possess practically identical unscaled frequency spectra, as previously shown in Fig. 6. Therefore, the unscaled frequency spectrum for both formulations is referred to as M-low in the following. We vary the amount of mass scaling and analyze the effect on the frequency spectra, see Fig. 8. Here, the absolute values of natural angular frequencies ω° are shown on the left and the ratio of scaled to unscaled natural angular frequencies ω°/ω are shown on the right. The scaling schemes from Eqs. (16) and (17) can be applied to both plate formulations, resulting in ISMS on transverse shear inertia for M-hr-low and in RMS on total rotational inertia for M-st-low, respectively.

The accuracy of the bending frequencies differs significantly for the two mass scaling schemes RMS and ISMS. When scaling the highest frequency by 50%, no significant differences between RMS and ISMS can be seen in the absolute frequencies of the bending branch in the left diagram. However, the relative representation in the right diagram already shows that the bending branch is captured with lower accuracy for RMS, while ISMS provides highly accurate results. This effect significantly increases

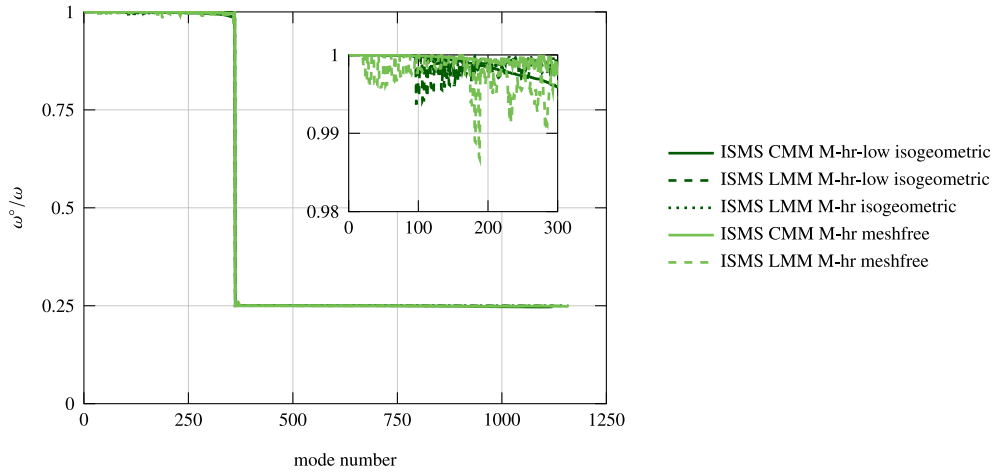

Fig. 9. Ratio of scaled to unscaled natural angular frequencies ω°/ω for **M-hr-low** with **isogeometric** discretization and for **M-hr** with **meshfree** discretization with **ISMS** using **CMM** and **LMM** and a reduction of the highest natural angular frequency by **75%** for slenderness $L/d = 100$.

when the maximum frequency is scaled by 75%, which demonstrates the superior accuracy of ISMS over RMS. At the same time, this indicates the potential for significant savings in computing time.

For the chosen problem setup, ISMS even enables a scaling of the maximum frequency by 85% or 90%. Then, however, it is necessary to take a closer look at the frequency spectra. The jump between bending branch and transverse shear branch is still clearly visible for a scaling level of 85%. For a scaling level of 90%, however, the bending frequencies and the transverse shear frequencies mix up within the spectrum, in which the calculated frequencies are sorted in ascending order. In fact, due to the strong scaling, some of the shear frequencies come to lie below the highest bending frequencies, which is not yet the case for a scaling level of 85%. This makes interpretations based on frequency spectra and, especially, on their relative representation no longer possible. Above all, this does not mean that the accuracy of bending frequencies is decreased. Instead, scaled transverse shear frequencies get meaninglessly related to unscaled bending frequencies. However, this mixing of frequencies only occurs for the ISMS M-hr 90% solution, which can be recognized by the preserved jump in the absolute frequency spectra for all other solutions. The conclusion made before, which relies on the relative representation and states that RMS already affects bending frequencies when using a scaling of 50%, still holds. In contrast to RMS, ISMS is able to keep frequencies of the bending branch mostly unaffected. Even for a scaling level of 85%, the relative representation shows only slightly deviating frequencies at the end of the bending branch.

In Fig. 9, we demonstrate that these results for ISMS' selective nature are not limited to a CMM and to an isogeometric discretization. We vary the type of the mass matrix and the discretization scheme for a scaling level, which reduces the maximum frequency by 75%. Independent of the type of mass matrix, that is CMM and LMM, ISMS is capable of selectively scaling the transverse shear branch, while the bending branch is practically unaffected. Therefore, the authors are confident that transferring ISMS to novel mass matrix types or lumping schemes will lead to highly accurate results as well. Furthermore, the discretization scheme can be chosen independently without influencing the effectivity and accuracy of ISMS.

A discretization with higher order B-Splines causes outlier frequencies in the frequency spectrum. In the following, we study the effects of higher polynomial degrees p and the effects of outlier frequencies on the accuracy of ISMS along with CMM and LMM. For this purpose, we analyze frequency spectra of the M-hr-low formulation without mass scaling and with ISMS and a scaling level of 50%. In Fig. 10, the unscaled frequencies ω and the scaled frequencies ω° are shown on the left, while the ratios of scaled to unscaled frequencies ω°/ω are shown on the right. As shown in [21], the accuracy of unscaled frequency spectra generally increases with higher polynomial degrees when using CMM. However, so-called outlier frequencies get progressively worse for higher degrees, which reduces the critical time step size in transient analyses. In the present study, outlier frequencies occur at the end of both the bending and the transverse shear branch. If ISMS is applied along with CMM, the outlier frequencies are scaled to the same extend as the other frequencies. Thus, the outliers of the transverse shear branch still limit the critical time step size. The bending frequencies are preserved by ISMS with high accuracy, even at higher polynomial degrees.

When using LMM, the quality of the unscaled frequencies decreases, as both the bending and shear frequencies are underestimated to a higher extent. For the chosen problem setup, however, no outlier frequencies are visible in the frequency spectra obtained by LMM, independent of the polynomial degree. This result is surprising and requires deeper studies in future work. In addition, in this particular problem setup, the bending and transverse shear branches are no longer separated for polynomial degrees $p \geq 4$. The missing separation of the two branches in the frequency spectrum leads to a mixing of the frequencies in the spectrum at polynomial degrees $p \geq 4$ due to the scaling of the transverse shear frequencies. Similar observations have been previously made for the very high scaling level of 90% using $p = 2$ and CMM, see Fig. 8. But, when using LMM, the bending frequencies are preserved by ISMS again with high accuracy, independent of the polynomial degree.

In general, the results from Fig. 10 show that the accuracy of ISMS for both LMM and CMM is not affected by higher degrees. As expected, ISMS is not able to remove the outlier frequencies of the transverse shear branch. In order to further exploit the potential

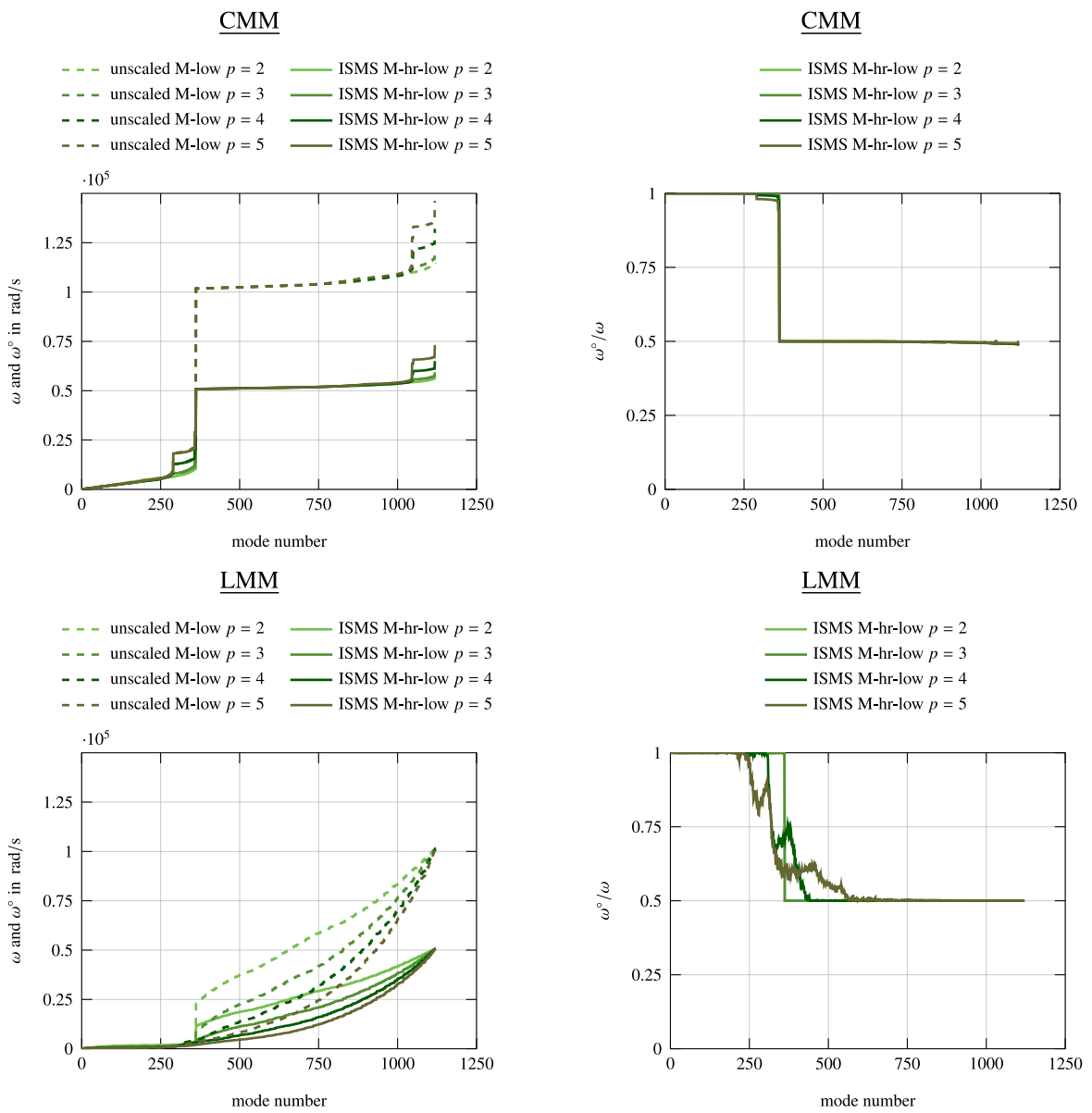

Fig. 10. Frequency spectra for **M-hr-low** with **ISMS** and a scaling level of 50% with **isogeometric** discretization for different polynomial degrees p using **CMM** and **LMM** and slenderness $L/d = 100$. Left: absolute values of natural angular frequencies ω and ω°. Right: ratio of scaled to unscaled natural angular frequencies ω°/ω.

of high critical time step sizes, the combination of ISMS and methods for outlier removal, see for instance [39], seem to be promising future developments.

To further demonstrate the high accuracy of ISMS, we perform a convergence study of the first two natural angular frequencies of the square plate problem from Fig. 5 (left) with hard simple support for CMM and LMM and for polynomial degrees $p = 2$ and $p = 3$. In Fig. 11, results are shown for both the unscaled case and for ISMS with a scaling level of 50%. For CMM both frequencies converge with the expected order of $2(p-1)$ to the analytical solution. The results for LMM are only second order accurate, independent of the chosen polynomial degree p, which is in line with results from literature, for instance [21]. In all cases, ISMS retains the accuracy and the expected convergence rates of the low frequencies.

The independence of both the type of mass matrix and the discretization scheme demonstrates that ISMS is indeed an *intrinsically* selective mass scaling scheme. This remarkable feature is mainly based on the clever reparametrization of kinematics within the hierarchic concept. In contrast to ISMS, RMS affects the total rotational mass, which decreases accuracy in the bending branch.

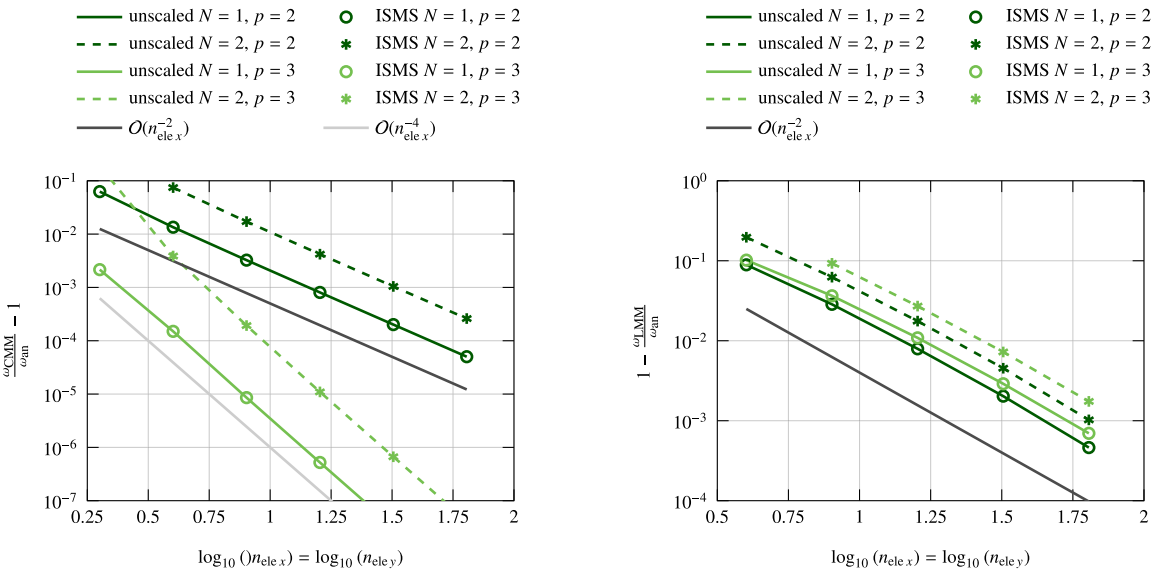

Fig. 11. Convergence of the first two natural angular frequencies using **M-hr-low** without mass scaling and with **ISMS** and a scaling level of 50% with **isogeometric** discretization for polynomial order $p = 2$ and $p = 3$ using slenderness $L/d = 100$. Left: **CMM**. Right: **LMM**.

4.4. Transient analyses

In the final subsection, we study the accuracy of ISMS in explicit transient analyses. We employ central differences [40] as explicit time integration scheme and study the plate problem shown in Fig. 5 with a soft support subject to a uniform surface load $p_z = 10d^3\,\text{MN/m}^2$ that lasts between $0 \leq t \leq 0.005\,\text{s}$. We consider two examples with different slenderness ratios, that is $L/d = 100$ and $L/d = 200$. We keep the side length $L = 10\,\text{m}$ constant and vary the plate's thickness accordingly, that is, $d = 0.1\,\text{m}$ and $d = 0.05\,\text{m}$. All other system and model parameters remain unchanged according to those shown in Fig. 5. All subsequent figures display the midpoint deflection over time.

In the first example, the plate's slenderness ratio is set to $L/d = 100$, for which bending and transverse shear frequencies can be clearly distinguished, as shown before. Here, we only show the results for the isogeometric discretization of the fully locking-free plate formulations M-st-low and M-hr-low using LMM. Corresponding frequency spectra for both the unscaled case and the case with mass scaling have been shown in Sections 4.2 and 4.3. Fig. 12 shows transient solutions for different levels of scaling. On the left, the maximum frequency of the discretized system is scaled by 75% and on the right by 90%. The main oscillation is dominated by the excitation of the first frequency, which is $\omega = 30.76\,\text{rad/s}$ for LMM. Additionally, higher bending frequencies are also excited as a result of the short loading duration. The curves for ISMS M-hr-low can hardly be distinguished from the corresponding curves obtained without mass scaling (unscaled M-low). This statement holds true for both scaling levels, coming along with a reduction of the number of time steps by 75% or by 90%, respectively. The results for RMS M-st-low show larger differences compared to the results for unscaled M-low. These differences are particularly pronounced for higher scaling factors, as can be seen from Fig. 12, right. Here, not only the peaks of the vibration amplitudes differ from the unscaled solution, but also the period is prolonged due to the increased mass.

For the second example, we consider a very thin plate with a slenderness ratio $L/d = 200$, for which the jump between the bending branch and the transverse shear branch in the frequency spectrum is very large. Therefore, up to 95.5% of the number of time steps and, thus, computational costs can be saved by utilizing a suitable mass scaling method. Fig. 13 shows transient solutions for the isogeometric discretization. The midpoint displacement is plotted over time for the plate formulations M-st-low and M-hr-low, both without and with mass scaling by RMS or ISMS, respectively. Furthermore, both mass matrix types CMM (left) and LMM (right) are employed. While RMS leads to large errors and, for the scaled LMM, to a strong phase shift, the results obtained using ISMS are almost identical to the results obtained without mass scaling, for both the CMM and LMM. Since RMS and ISMS do not increase the number of non-zero entries in the mass matrix and, thus, the computational costs for the solution in a single time step remain unchanged in case direct solvers are used, the gain of efficiency obtained by RMS/ISMS is directly proportional to the increase of the allowed critical time step size. This means, that for this example ISMS facilitates a speedup of the computation by a factor of 200 is possible, without a perceivable effect on accuracy.

Next, the same problem is studied using a meshfree discretization and corresponding results are shown in Fig. 14. The midpoint displacement using unscaled mass matrices differs for M-st and M-hr due to locking effects. Therefore, the results for both formulations, which were obtained with scaled mass matrices, are compared with the corresponding unscaled results. The results for RMS M-st obtained by the meshfree discretization are slightly better than the ones obtained by the isogeometric discretization. But again, the superior accuracy of ISMS compared to RMS is clearly visible for both mass matrices.

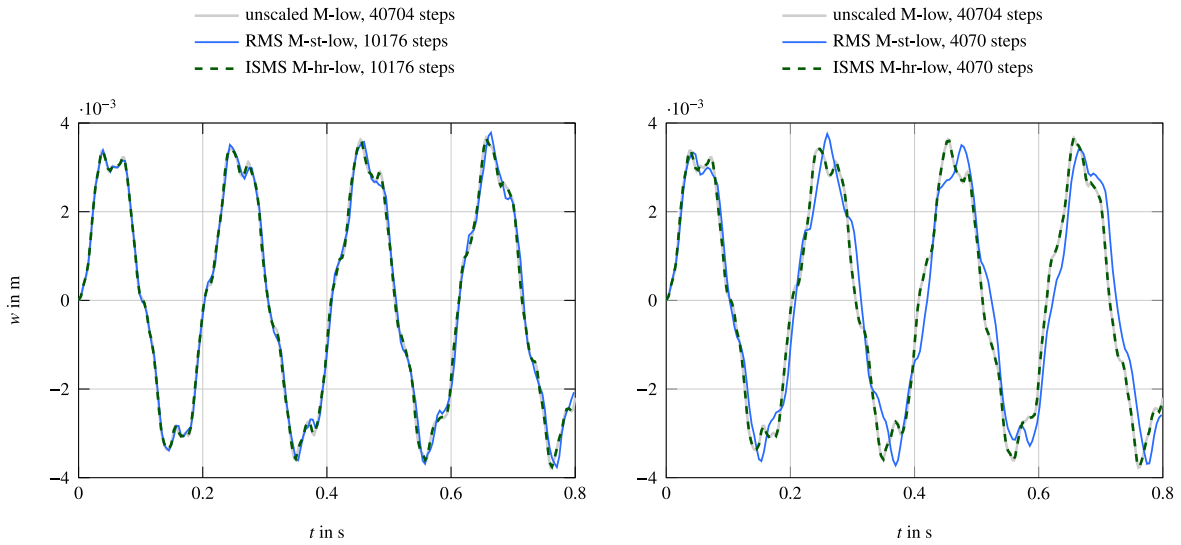

Fig. 12. Midpoint displacement history using unscaled and scaled **LMM** for slenderness $L/d = 100$ and an **isogeometric** discretization. Left: reduction of the highest natural angular frequency by **75%**. Right: reduction of the highest natural angular frequency by **90%**.

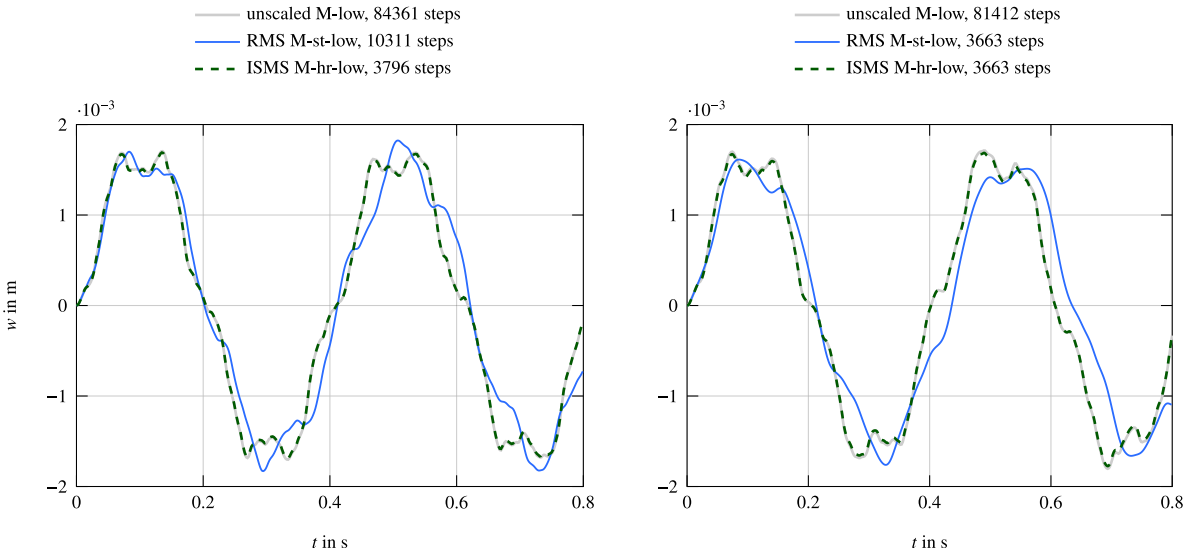

Fig. 13. Midpoint displacement history for slenderness $L/d = 200$ using an **isogeometric** discretization and a reduction of the highest natural angular frequency by **95.5%** (except RMS CMM M-st-low: by **87.7%**) for the scaled mass matrices. Left: using **CMM**. Right: using **LMM**.

For both discretizations, RMS applied to CMM for M-st-low and M-st does not allow a reduction of the highest frequency by 95.5%, but ISMS does. But even with a smaller reduction by 87.7% for the isogeometric discretization or 88.0% for the meshfree discretization, the results for RMS show lower accuracy than for ISMS. In this extreme situation with high slenderness ratio and high scaling factors, the differences between RMS and ISMS become clearly visible. Due to its intrinsic properties, ISMS is highly accurate and outperforms RMS for both CMM and LMM and for both discretization schemes, that is an isogeometric and the meshfree discretization.

5. Conclusion and outlook

In this paper, the concept of *intrinsically selective mass scaling (ISMS)* has been presented for hierarchic plate formulations. The key to ISMS is the employment of the positive properties of hierarchic structural element formulations. Thus, it is not readily transferable to other element types, like standard solid elements. The hierarchic formulations are intrinsically free from transverse shear locking and possess distinct transverse shear variables within a pure primal formulation. This enables a direct, selected access of transverse

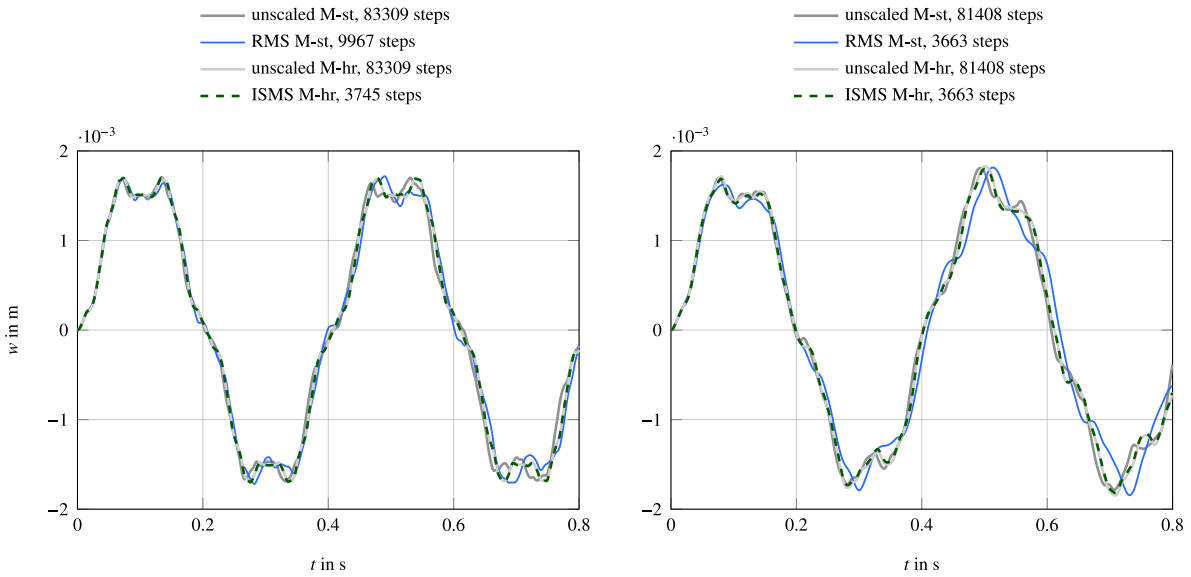

Fig. 14. Midpoint displacement history for slenderness $L/d = 200$ using a **meshfree** discretization and a reduction of the highest natural angular frequency by **95.5%** (except RMS CMM M-st: by **88.0%**) for the scaled mass matrices. Left: using **CMM**. Right: using **LMM**.

shear frequencies, while bending frequencies remain mostly unaffected. A formulation that also avoids membrane locking is still pending.

We studied the performance of ISMS for both CMMs and LMMs and for both an isogeometric discretization scheme based on B-splines and a meshfree discretization scheme based on maximum-entropy approximants. Numerical results for both spectral and transient problems confirm that ISMS possesses a high potential of increasing computational efficiency in explicit dynamics. At the same time, ISMS solutions preserve the accuracy of the unscaled solution, independent of a particular type of mass matrix and independent of a particular discretization scheme.

Due to its simple structure and its promising properties, the ISMS concept has the potential to be applied to any smooth discretization of shear-deformable beam, plate and shell models. The only requirement for the application of ISMS is the implementation of hierarchic shear-deformable structural element formulations. ISMS naturally preserves both linear and angular momentum and preserves the diagonality of lumped mass matrices, while being as simple as RMS. This particular property may enable further efforts towards efficient and simultaneously accurate (selective) mass scaling schemes in the context of IGA and other smooth discretization schemes.

Since row-sum lumping is only second order accurate within IGA, the development of more accurate lumped mass matrices for hierarchic formulations is of high interest in the future. Alternative lumping schemes may also be the key to make the hierarchic displacement formulation accessible to intrinsically selective mass scaling. This would be particularly attractive, because the hierarchic rotation formulation used in all examples in this paper still suffers from some oscillations that are not present in the hierarchic displacement formulation. In future work, the extension of ISMS to hierarchic shear deformable large rotation shell formulations, see [16,41], and nonlinear transient analyses is necessary. For a practical application of ISMS, investigations on optimal scaling parameters and developments of efficient and accurate time step estimates are crucial, as discussed in Section 3.2.

CRediT authorship contribution statement

Lisa-Marie Krauß: Writing – review & editing, Writing – original draft, Software, Methodology, Investigation, Formal analysis, Conceptualization. **Rebecca Thierer:** Writing – review & editing, Writing – original draft, Software, Methodology, Investigation, Conceptualization. **Manfred Bischoff:** Writing – review & editing, Supervision, Resources, Conceptualization. **Bastian Oesterle:** Writing – review & editing, Writing – original draft, Supervision, Software, Methodology, Investigation, Funding acquisition, Conceptualization.

Declaration of competing interest

The authors declare the following financial interests/personal relationships which may be considered as potential competing interests: Bastian Oesterle reports financial support was provided by German Research Foundation. If there are other authors, they declare that they have no known competing financial interests or personal relationships that could have appeared to influence the work reported in this paper.

Data availability

Data will be made available on request.

Acknowledgments

This project is supported by the Deutsche Forschungsgemeinschaft (DFG, German Research Foundation) under Grant OE 728/1-1 – 428725889. This support is gratefully acknowledged.

References

[1] C.A. Felippa, Q. Guo, K.C. Park, Mass matrix templates: General description and 1D examples, Arch. Comput. Methods Eng. 22 (2015) 1–65, http://dx.doi.org/10.1007/s11831-014-9108-x.
[2] L. Olovsson, K. Simonsson, M. Unosson, Selective mass scaling for explicit finite element analyses, Internat. J. Numer. Methods Engrg. 63 (10) (2005) 1436–1445, http://dx.doi.org/10.1002/nme.1293.
[3] A. Tkachuk, M. Bischoff, Variational methods for selective mass scaling, Comput. Mech. 52 (2013) 563–570, http://dx.doi.org/10.1007/s00466-013-0832-0.
[4] T.J.R. Hughes, M. Cohen, M. Haroun, Reduced and selective integration techniques in the finite element analysis of plates, Nucl. Eng. Des. 46 (1) (1978) 203–222, http://dx.doi.org/10.1016/0029-5493(78)90184-X.
[5] T. Belytschko, W.L. Mindle, Flexural wave propagation behavior of lumped mass approximations, Comput. Struct. 12 (6) (1980) 805–812, http://dx.doi.org/10.1016/0045-7949(80)90017-6.
[6] R. Echter, B. Oesterle, M. Bischoff, A hierarchic family of isogeometric shell finite elements, Comput. Methods Appl. Mech. Engrg. 254 (2013) 170–180, http://dx.doi.org/10.1016/j.cma.2012.10.018.
[7] B. Oesterle, E. Ramm, M. Bischoff, A shear deformable, rotation-free isogeometric shell formulation, Comput. Methods Appl. Mech. Engrg. 307 (2016) 235–255, http://dx.doi.org/10.1016/j.cma.2016.04.015.
[8] B. Oesterle, S. Bieber, R. Sachse, E. Ramm, M. Bischoff, Intrinsically locking–free formulations for isogeometric beam, plate and shell analysis, Proc. Appl. Math. Mech. 18 (1) (2018) http://dx.doi.org/10.1002/pamm.201800399.
[9] B. Oesterle, J. Trippmacher, A. Tkachuk, M. Bischoff, Intrinsically selective mass scaling with hierarchic structural element formulations, in: Book of Extended Abstracts of the 6th ECCOMAS Young Investigators Conference, 7th-9th July 2021, Valencia, Spain, 2021, pp. 99–108, http://dx.doi.org/10.4995/YIC2021.2021.12418.
[10] R.D. Mindlin, Influence of rotatory inertia and shear on flexural motions of isotropic, elastic plates, J. Appl. Mech. 18 (1) (1951) 31–38, http://dx.doi.org/10.1115/1.4010217.
[11] G. Kirchhoff, Über das gleichgewicht und die bewegung einer elastischen scheibe, J. Reine Angew. Math. (Crelles J.) 1850 (40) (1850) 51–88, http://dx.doi.org/10.1515/crll.1850.40.51.
[12] J.N. Reddy, Theory and Analysis of Elastic Plates, second ed., CRC Press, Philadelphia, 2006, http://dx.doi.org/10.1201/9780849384165.
[13] W. Soedel, third ed., Vibrations of Shells and Plates, vol. 177, CRC Press, New York, 2004, http://dx.doi.org/10.4324/9780203026304.
[14] E. Hinton (Ed.), Numerical Methods and Software for Dynamic Analysis of Plates and Shells, first ed., Pineridge Press, Swansea, 1988.
[15] C.M. Wang, Natural frequencies formula for simply supported Mindlin plates, J. Vib. Acoust. 116 (4) (1994) 536–540, http://dx.doi.org/10.1115/1.2930460.
[16] B. Oesterle, R. Sachse, E. Ramm, M. Bischoff, Hierarchic isogeometric large rotation shell elements including linearized transverse shear parametrization, Comput. Methods Appl. Mech. Engrg. 321 (2017) 383–405, http://dx.doi.org/10.1016/j.cma.2017.03.031.
[17] L. Beirão Da Veiga, T.J.R. Hughes, J. Kiendl, C. Lovadina, J. Niiranen, A. Reali, H. Speleers, A locking-free model for Reissner–Mindlin plates: Analysis and isogeometric implementation via NURBS and triangular NURPS, Math. Models Methods Appl. Sci. 25 (08) (2015) 1519–1551, http://dx.doi.org/10.1142/S0218202515500402.
[18] Q. Long, P. Burkhard Bornemann, F. Cirak, Shear-flexible subdivision shells, Internat. J. Numer. Methods Engrg. 90 (13) (2012) 1549–1577, http://dx.doi.org/10.1002/nme.3368.
[19] J.-L. Batoz, E. Antaluca, I. Katili, On the formulation and evaluation of old and new efficient low order triangular plate bending elements with shear effects, Comput. Mech. 68 (2021) 69–96, http://dx.doi.org/10.1007/s00466-021-02020-6.
[20] L. Beirão da Veiga, A. Buffa, C. Lovadina, M. Martinelli, G. Sangalli, An isogeometric method for the Reissner–Mindlin plate bending problem, Comput. Methods Appl. Mech. Engrg. 209–212 (2012) 45–53, http://dx.doi.org/10.1016/j.cma.2011.10.009.
[21] J.A. Cottrell, A. Reali, Y. Bazilevs, T.J.R. Hughes, Isogeometric analysis of structural vibrations, Comput. Methods Appl. Mech. Engrg. 195 (41–43) (2006) 5257–5296, http://dx.doi.org/10.1016/j.cma.2005.09.027.
[22] E. Hinton, T. Rock, O.C. Zienkiewicz, A note on mass lumping and related processes in the finite element method, Earthq. Eng. Struct. Dyn. 4 (3) (1976) 245–249, http://dx.doi.org/10.1002/eqe.4290040305.
[23] G.C. Archer, T.M. Whalen, Development of rotationally consistent diagonal mass matrices for plate and beam elements, Comput. Methods Appl. Mech. Engrg. 194 (6–8) (2005) 675–689, http://dx.doi.org/10.1016/j.cma.2003.08.015.
[24] Y. Yang, H. Zheng, M.V. Sivaselvan, A rigorous and unified mass lumping scheme for higher-order elements, Comput. Methods Appl. Mech. Engrg. 319 (2017) 491–514, http://dx.doi.org/10.1016/j.cma.2017.03.011.
[25] C. Anitescu, C. Nguyen, T. Rabczuk, X. Zhuang, Isogeometric analysis for explicit elastodynamics using a dual-basis diagonal mass formulation, Comput. Methods Appl. Mech. Engrg. 346 (2019) 574–591, http://dx.doi.org/10.1016/j.cma.2018.12.002.
[26] Y. Voet, E. Sande, A. Buffa, A mathematical theory for mass lumping and its generalization with applications to isogeometric analysis, Comput. Methods Appl. Mech. Engrg. 410 (2023) 116033, http://dx.doi.org/10.1016/j.cma.2023.116033.
[27] T.-H. Nguyen, R.R. Hiemstra, S. Eisenträger, D. Schillinger, Towards higher-order accurate mass lumping in explicit isogeometric analysis for structural dynamics, Comput. Methods Appl. Mech. Engrg. (2023) 116233, http://dx.doi.org/10.1016/j.cma.2023.116233.
[28] S. Held, S. Eisenträger, W. Dornisch, An efficient mass lumping scheme for isogeometric analysis based on approximate dual basis functions, Tech. Mech. - Eur. J. Eng. Mech. 44 (2024) 14–46, http://dx.doi.org/10.24352/UB.OVGU-2024-052, Number: 1.
[29] L. Radtke, M. Torre, T.J. Hughes, A. Düster, G. Sangalli, A. Reali, An analysis of high order FEM and IGA for explicit dynamics: Mass lumping and immersed boundaries, Internat. J. Numer. Methods Engrg. 125 (16) (2024) e7499, http://dx.doi.org/10.1002/nme.7499.
[30] S. Hartmann, D.J. Benson, Mass scaling and stable time step estimates for isogeometric analysis, Internat. J. Numer. Methods Engrg. 102 (3–4) (2014) 671–687, http://dx.doi.org/10.1002/nme.4719.
[31] D.J. Benson, Y. Bazilevs, M.-C. Hsu, T.J.R. Hughes, Isogeometric shell analysis: The Reissner–mindlin shell, Comput. Methods Appl. Mech. Engrg. 199 (5–8) (2010) 276–289, http://dx.doi.org/10.1016/j.cma.2009.05.011.
[32] L. Leidinger, M. Breitenberger, A. Bauer, S. Hartmann, R. Wüchner, K.-U. Bletzinger, F. Duddeck, L. Song, Explicit dynamic isogeometric B-Rep analysis of penalty-coupled trimmed NURBS shells, Comput. Methods Appl. Mech. Engrg. 351 (2019) 891–927, http://dx.doi.org/10.1016/j.cma.2019.04.016.

[33] B. Oesterle, A. Tkachuk, M. Bischoff, Finite element technology-based selective mass scaling for shear deformable structural element formulations, in: COMPDYN 2023, 9th ECCOMAS Thematic Conference on Computational Methods in Structural Dynamics and Earthquake Engineering, M. Papadrakakis, M. Fragiadakis (Eds.), Athens, Greece, 12-14 June 2023, 2023, pp. 1965–1973, http://dx.doi.org/10.7712/120123.10534.20662.
[34] D.J. Benson, Explicit finite element methods for large deformation problems in solid mechanics, in: Encyclopedia of Computational Mechanics Second Edition, John Wiley & Sons, Ltd, 2017, pp. 1–43, http://dx.doi.org/10.1002/9781119176817.ecm2072.
[35] T.J.R. Hughes, J.A. Cottrell, Y. Bazilevs, Isogeometric analysis: CAD, finite elements, NURBS, exact geometry and mesh refinement, Comput. Methods Appl. Mech. Engrg. 194 (39–41) (2005) 4135–4195, http://dx.doi.org/10.1016/j.cma.2004.10.008.
[36] J.A. Cottrell, T.J.R. Hughes, Y. Bazilevs, Isogeometric Analysis: Toward Integration of CAD and FEA, Wiley, Chichester, West Sussex, U.K., 2009, http://dx.doi.org/10.1016/j.cma.2005.09.027.
[37] M. Arroyo, M. Ortiz, Local maximum-entropy approximation schemes: a seamless bridge between finite elements and meshfree methods, Internat. J. Numer. Methods Engrg. 65 (13) (2006) 2167–2202, http://dx.doi.org/10.1002/nme.1534.
[38] C.J. Cyron, M. Arroyo, M. Ortiz, Smooth, second order, non-negative meshfree approximants selected by maximum entropy, Internat. J. Numer. Methods Engrg. 79 (13) (2009) 1605–1632, http://dx.doi.org/10.1002/nme.2597.
[39] R.R. Hiemstra, T.J.R. Hughes, A. Reali, D. Schillinger, Removal of spurious outlier frequencies and modes from isogeometric discretizations of second- and fourth-order problems in one, two, and three dimensions, Comput. Methods Appl. Mech. Engrg. 387 (114115) (2021) 114115.
[40] T. Belytschko, K. Liu, B. Moran, K. Elkhodary, Nonlinear Finite Elements for Continua and Structures, second ed., John Wiley & Sons, Nashville, TN, 2013.
[41] R. Thierer, B. Oesterle, E. Ramm, M. Bischoff, Transverse shear parametrization in hierarchic large rotation shell formulations, Internat. J. Numer. Methods Engrg. 125 (2024) http://dx.doi.org/10.1002/nme.7443.